Atmos. Meas. Tech. Discuss., 6, 10165–10189, 2013
www.atmos-meas-tech-discuss.net/6/10165/2013/
doi:10.5194/amtd-6-10165-2013

Atmospheric Measurement Techniques Discussions

A video precipitation sensor for imaging and velocimetry of hydrometeors

X. C. Liu, T. C. Gao, and L. Liu

College of Meteorology and Oceanography, PLA University of Science and Technology, Nanjing, China

Received: 15 October 2013 – Accepted: 22 November 2013 – Published: 29 November 2013

Correspondence to: T. C. Gao (2009gaotc@gmail.com)

Published by Copernicus Publications on behalf of the European Geosciences Union.

Abstract

A new method to determine the shape and fall velocity of hydrometeors by using a single CCD camera is proposed in this paper, and a prototype of Video Precipitation Sensor (VPS) is developed. The instrument consists of an optical unit (collimated light source with multi-mode fiber cluster), an imaging unit (planar array CCD sensor), an acquisition and control unit, and a data processing unit, the cylindrical space between the optical unit and imaging unit is sampling volume (300 mm × 40 mm × 30 mm). As the precipitation particles fall through the sampling volume, the CCD camera exposures two times in a single frame, by which the double-exposure of particles images can be obtained. The size and shape can be obtained by the images of particles; the fall velocity can be calculated by particle displacement in double-exposure image and interval time; the drop size distribution and velocity distribution, precipitation intensity, and accumulated precipitation amount can be calculated by time integration. The innovation of VPS is that the shape, size, and velocity of precipitation particles can be measured by only one planar array CCD sensor, which can address the disadvantages of linear scan CCD disdrometer and impact disdrometer. Field measurements of rainfall demonstrate the VPS's capability to measure micro-physical properties of single particles and integral parameters of precipitation.

1 Introduction

The needs for detailed knowledge on precipitation microstructures in the fields of precipitation remote sensing, terrestrial and satellite radio transmission, tropospheric wave propagation, and other atmospheric sciences and applications motivate the continuing development of various disdrometers. Joss–Waldvogel disdrometer (Joss and Waldvogel, 1967; Liu et al., 2013), OTT PARSIVEL disdrometer (Löffler-Mang and Joss, 2000), 2D Video Disdrometer (2DVD) (Kruger and Krajewski, 2002), Hydrometeor Velocity and Shape Detector (HVSD) (Barthazy et al., 2004), and Snowflake Video

AMTD
6, 10165–10189, 2013

Imager (SVI) (Newman and Kucera, 2009) are by far the most widely applied instruments for precipitation microstructures, but each instrument has its own advantages and limitations due to its measurement principle.

The Joss–Waldvogel disdrometer infers the size of each raindrop from the measured impact kinetic energy of the raindrop based on an empirical nonlinear assumption between fall velocity and raindrop diameter (Joss and Waldvogel, 1967, 1977), but it cannot measure the velocity and shape of raindrops. OTT PARSIVEL disdrometer can measure the horizontal size of particles by using a decrease of light signal by extinction; the vertical size and fall velocity of particles are estimated by the empirical assumption of raindrops' shape (Löffler-Mang and Joss, 2000), but the difference between assumption and real rainfall can cause an distortion of raindrop size and velocity distribution. And it cannot measure the particles' shapes (Battaglia et al., 2010).

Both 2DVD (Schonhuber et al., 2007) and HVSD (Barthazy et al., 2004) have two line-scan cameras, the vertical velocity of each drop can be calculated according to its traveling time and the distance between two light sheets (Schonhuber et al., 2007). 2DVD can measure three-dimensional shapes of the raindrops, while HVSD can only measure two-dimensional shapes of the raindrops. Since the raindrop's image is acquired in sequential planar sections as it falls through the light sheet, horizontal motion of the droplet in the presence of horizontal winds resulting in a distorted image of the raindrop. While corrections for this exist, errors in the drop shape measurement remain (Tokay et al., 2001; Saylor et al., 2002). SVI can measure the shapes and size distributions of snowflakes by using a CCD image sensor illuminated by a halogen flood lamp (Newman and Kucera, 2009). Rain Imaging System (RIS) used the similar principle (Saylor et al., 2002; Jones et al., 2003; Saylor and Sivasubramanian, 2007), but they cannot measure the fall velocity of snowflakes/raindrops.

This paper presents a new ground-based Video Precipitation Sensor (VPS) for imaging and velocimetry of hydrometeors; it can measure the shape, size, orientation, and fall velocity of naturally falling hydrometeors simultaneously by using a planar array CCD camera with exposure controlled precisely, which represents a promising

AMTD
6, 10165–10189, 2013

alternative to monitor precipitation particles. From these rain rate, rain accumulation, drop size distribution, drop velocity distribution, and other precipitation-related variables can be estimated. The following sections contain descriptions of the instrument VPS, of the image processing and feature extraction algorithms, of the results of calibration and field experiments. The last part summarizes the main features and future work of VPS.

2 The VPS system

2.1 Main components

The VPS consists of four units: optical unit, imaging unit, acquisition and control unit, and data processing unit, as shown in Fig. 1a. The optical unit and imaging unit are integrated into one tunnel housing, on which there are a couple of metal splash elimination grids, to prevent raindrops splashing into the sampling area and minimize the wind disturbances of the instruments, as shown in Fig. 1b. The sampling size between the optical unit and imaging unit is 300 mm × 40 mm × 30 mm.

The optical unit contains a multi-mode fiber cluster, expanded beam lens, and concentration lens, which provide a parallel light beam for imaging unit; considering that small particles illuminated by laser light will create diffraction patterns, the incoherent light (λ = 460 nm) from LED is used in this system, and the multi-mode fiber cluster are used to concentrate the light and increase the light intensity. To address the depth of field in imaging system, we design a telecentric afocal imaging system, as shown in Fig. 2. The chief ray is parallel to the axis in object space and image space, and both the EP and the XP are located at infinity, which ensure that the image size does not change with focus position. The centered lens are used to generate the parallel light beam, the divergence is less than 0.2 mrad.

The imaging unit contains one charge-coupled device (CCD) image sensor and one matching driving circuit, the CCD image sensor has 640 pixels × 480 pixels in interlaced

AMTD
6, 10165–10189, 2013

mode; we operated it in 640 pixels × 240 pixels noninterlaced mode (50 frames per second). The single exposure time is 20 µm so blurring that particle motion is insignificant, and the time between two exposures is 2 ms so that the two exposures of the same particle can be recorded in one image. The superiority of the CCD camera is that images can be obtained almost instantaneously and thus there's no need to correct the particle movement.

Acquisition and control unit contains a digital signal processor (DSP, C6000 series, TMS320DM642), a complex programmable logic device (CPLD, MachX0 series, LCMX0256), Ethernet driver chips (LXT971ALC), reset circuit, clock circuit, storage chips and other support integrated circuits, which controls the optical unit and imaging unit, records and preprocesses the raw images, encodes and transmits the raw data. Data processing unit is an PC terminal that communicates with the acquisition and control unit using a coaxial network cable via the Internet TCP/IP protocol. Software running on the terminal receives the data obtained by the sensor, processes the hydrometeors' images, and calculates the size, velocity, and shape of hydrometeors.

2.2 Principle of operation

The optical unit generates a cylindrical light beam that is projected onto the CCD image sensor with a special driving circuit. The light beam is so bright that the VPS is insensitive to ambient light, precipitation particles falling through the light beam shadow render the opaque of precipitation particles, which are recorded by the CCD sensor; the images are compared against a gray scale threshold (determined by calibration) to determine whether each pixel of images is lit or obscured. The CCD sensor has a resolution of 640 pixels × 240 pixels, the corresponding field of view is 40 mm × 30 mm, and hence each pixel size of an image is 0.0625 mm (horizontal) × 0.125 mm (vertical). The CCD sensor runs in 50 fps, a pulse synchronous signal generator is used to generate two exposures in each frame, the interval of two exposures is 2 ms. The timing sequence of exposure and images recorded by VPS are shown in Fig. 3.

AMTD
6, 10165–10189, 2013

The CCD sensor records the double-exposure image of each particle in a single frame, by which the two-dimensional particle shape information can be obtained, and the size, volume, equivalent diameter, as well as oblateness of particles can be calculated by the image processing algorithm. Each particle is exposed twice in a single frame, its displacement can be calculated according to the location of two exposed images, hence the vertical and horizontal velocity of each particle can be calculated according to its displacement and exposure interval. The drop size distribution and drop velocity distribution can be obtained by the time integration, by which the intensity, amount, and type of precipitation can be estimated.

Preliminary experiments found that there are certain noises in the background of image due to the optical lens polluted by dust, dew, or frost in the natural environment, light intensity might change due to the instability of light source in the long-time running, therefore a real-time adaptive averaging method is designed to remove the background of image, which has been embedded in the DSP software. Considering that the sampling rate of VPS is 50 fps, the maximum data of original images might reach 25.7 GB in 1 h, which is a great challenge to the computer storage. To minimize the data sizes, an encoding method for original images is proposed, there are only minimum enclosing rectangles (MER) around the raindrops images are saved and transmitted to the data processing unit. The flowchart of background removing and encoding is shown in Fig. 4, the detail processes are: (i) original images are stored in the cache; (ii) each 1024 frame images are averaged as a background of image; (iii) original images are subtracted by the background; (iv) the available images of particles are detected and transmitted to the data processing terminal.

AMTD
6, 10165–10189, 2013

3 Data processing algorithm

3.1 Image processing

The CCD sensor has a resolution of 640 pixels × 240 pixels, the corresponding field of view is 40 mm × 30 mm, and hence the minimum particle (0.1 mm) has 1.6 pixels in horizontal direction and 0.8 pixels in vertical direction theoretically. Preliminary imaging experiments found that there are image diffusions due to the defocusing of imaging system, which causes the overestimation of particle size. We propose an image restoration algorithm based on point spread function (PSF), considering that the motion blur of particles is insignificant, the defocusing blur is the main factor for images degradation, in which the PSF can be defined as:

$$h(i,j) = \begin{cases} 1/(\pi R^2) & \sqrt{i^2+j^2} \le R \\ 0 & \sqrt{i^2+j^2} > R \end{cases} \quad (1)$$

where the R is the defocusing radius.

Figure 5 shows the flowchart of images processing and feature extraction. The image processing begins with a median filter algorithm (step 1), to remove the noises and obtain the filtered images; next the PSF (step 2) is applied to restore the filtered images; then the binarization algorithm (step 3) is used to obtain the binary images; the edge detection algorithm (step 4) is used to detect the edges and obtain the contour of particles; at last the size detection algorithm (step 5) is used to calculate the horizontal size, vertical size, equivolumetric diameter, axis ratio, orientation, and etc.

We validated the image processing algorithm using glass balls (10 sizes ranging in diameter from 1 to 4.5 mm), which have the similar refractive index with the water drops. Figure 6 shows the results of image processing (D = 2 mm); it shows that this algorithm can obtain the sharp image and clear edge of particles, so the VPS and analysis software can provide precise measurements for the size, shape, orientation, velocity of particles.

AMTD
6, 10165–10189, 2013

3.2 Feature extraction

Considering the operation principle of VPS, the effective sampling time is only 10 % of the exposure time of each frame; therefore not every particle that passes through the sampling area can be imaged by CCD. The probability that a certain particle with a certain size and fall velocity can be captured by the camera is defined as (so-called capture probability)

$$\mathrm{Prob}(D) = \frac{H - D_V - V(D) \cdot T_{\mathrm{interval}}}{V(D) \cdot 20\,\mathrm{ms}} \quad (2)$$

where H is the height of sampling size, D_V is the vertical size of drops, $V(D)$ is the vertical velocity of drops, T_{interval} is the exposure interval in each frame, 20 ms is the exposure time of each frame. It can be found that different particles have different capture probabilities.

The raindrop size distribution $N(D)$ can be computed as follows:

$$N(D) = \frac{\mathrm{Num}(D)}{\mathrm{Vol} \cdot \mathrm{dD} \cdot \mathrm{Prob}(D)} \quad (3)$$

where $N(D)$ is the sampled number concentration of particles per volume per size ($\mathrm{m}^{-3}\,\mathrm{mm}^{-1}$); Num($D$) is the number of particles of each bin, which can be obtained by counting particles and summing volume increments during the time interval (1 min in this system); Vol is the effective sampling volume; dD is the interval size of particle, which equals to 0.2 mm for 50 bins spanning from 0.1 to 10 mm; Prob(D) is the capture probability of a raindrop with diameter D, "V" in Eq. (2) is the average velocity for each particle size bin.

Rain rate (R) is calculated by the integration of drop size distribution $N(D)$, velocity distribution $V(D)$, equivolumetric diameter D, and density ρ:

$$R = \frac{\pi}{6} \int_0^{\infty} N(D) \rho D^3 V(D) \mathrm{dD}. \quad (4)$$

AMTD
6, 10165–10189, 2013

4 Calibration

The VPS fundamentally takes photographs of precipitation particles when they pass through the sampling volume, it infers horizontal and vertical dimensions of particles from the images, and the estimation of particle velocity is independent from the particle shape, therefore the size of particles are the only required data for calibration. The telecentric imaging lens designed in VPS infers that the depth of field (DOF) of VPS is infinite; therefore a single particle falling at different distances from the center of focus can be recorded as the same size of images. However, the light source in VPS system is not the ideal point light source, the defocusing blurred images are larger than the real sizes; therefore a proper defocusing radius of PSF and a binarization threshold are crucial to the successful operation of VPS.

Preliminary test of the point light source has determined that the defocusing radius of PSF is 5 pixels; hence the determination of gray scale threshold is a critical part of calibration. It is clear that if the binarization threshold is high, the VPS underestimates particle sizes; whereas if the threshold is low, the VPS overestimates the sizes. In this paper, VPS is calibrated by dropping small glass balls (10 sizes ranging from 1 mm to 4.5 mm in diameter) through the sampling area.

Figure 7 shows the result of calibration images by a fixed threshold (3 %); note that if we set a fixed gray scale threshold for different sizes of particles, there would be significant error for particles' size, rain rate and accumulated rain amount. Therefore we use different thresholds for different sizes of particles, the calibrated threshold vs. diameter can be approximated using a linear fit, as shown in Fig. 8. This is useful since, in a field operation, it provide a means for determining the size of each particle size accurately.

AMTD
6, 10165–10189, 2013

5 Field measurement

A VPS system was located at Nanjing, China, during May 2013, by which several rainfall events have been observed. 39 218 frames of images were recorded from 23:00 to 24:00 UTC on 8 May 2013, in which 6317 images of raindrops were recorded, and hence the overall capture probability is 16.1 %. A sample of images of raindrops in free fall taken by VPS is illustrated in Fig. 9, it can be found that the images have sharp edge and contour, by which the shape, horizontal size, and vertical size can be calculated precisely.

Figure 10 shows the distributions for fall velocity (a), axis ratio (b), and canting angle (c) of raindrops. Considering that the rain rate is only 2.5 mm h^{-1} (measured by rain gauge), this rainfall is mainly dominated by small drops ($D_{eq} < 2$ mm), and the maximum diameter is 2.3 mm. The fall velocity of raindrops increase obviously with the increasing of the diameter, and the observed data are in good agreement with the empirical velocity relationship proposed by Atlas (Atlas and Ulbrich, 1977). It should be noted that there are a certain number of velocity outliers of raindrops measured by the VPS, in which some large raindrops have small velocities, and some small raindrops have large velocities beyond empirical values. The possible reason is that there was a strong wind with speed > 8 m s^{-1}, wind blow or turbulence might cause the deviation of normal fall velocity. And another possible explanation is splashing where one drop hits the side of VPS and a part of it passes through the measuring area.

Many researchers have studied the relationships between the axis ratio and the diameter of raindrops by theoretical analysis, laboratory measurement and field measurement; several relationships have been proposed (Beard and Chuang, 1987; Chandrasekar et al., 1988; Andsager et al., 1999; Thurai et al., 2009; Marzuki et al., 2013). The observed axis ratio of large raindrops have an obvious correlation with the empirical relationship by Pruppacher and Beard (Pruppacher and Beard, 1970), while the axis ratio of small raindrops show a much wider dispersion. Considering that the axis ratio of small raindrops ($D_{eq} < 1$ mm) is greater than 0.96, the oblateness of large

AMTD
6, 10165–10189, 2013

raindrops is the focus of research. We will observe more large raindrops and study the axis ratio distribution of raindrops in future field experiment.

The canting angle (so-called orientation) is the angle between the projection of the drop's symmetry axis and the projection of the "true" local vertical direction, which have a certain influence on the polar radar measurements (Huang et al., 2008). Figure 10c shows the canting angle distribution, note that the mean canting angle is nearly 2.1°, with the standard deviation close to 11.5°, which is greater than the results of 80 m fall artificial rainfall by 2DVD, the possible reason is that there was a strong wind (larger than 8 $m s^{-1}$) at that time, causing a much wider variation.

The VPS recorded a rainfall event from 8 May 2013 21:00 UTC, to 9 May 2013 04:00 UTC, the time history of raindrops number per minute, rain rate, and raindrop size distribution are shown in Fig. 11. The rain gauge reported a total rain amount of 2.5 mm. During the event, the VPS recorded 157 694 frames of images, in which there were 26 566 images of raindrops; the average is about 63 raindrops per minute, and overall capture probability is 16.8 %. The maximum raindrops number per minute was 1333 occurred during 00:25 UTC, whereas the rainfall have not the strongest rain rate, the reason is that small raindrops are in the majority, which contribute little to rain rate, it can be validated by the Drop Size Distribution in Fig. 11c. The VPS frame rate is 50 fps, so about 1 in 47 frames had a couple of double-exposure raindrops. We conclude that the VPS yields a sufficient number of particles for hydrometeors micro-physical characteristics studies.

6 Conclusions

An innovative ground-based optical instrument, the Video Precipitation Sensor (VPS), is developed to measure the detailed information of free falling precipitation particles in natural environment, which provides a promising alternative to monitor precipitation particles. It is a low-cost instrument and requires minimal maintenance for the long-lasting running in the wild.

AMTD
6, 10165–10189, 2013

The VPS has one horizontal cylindrical parallel light beam (300 mm × 40 mm × 30 mm), the double-exposure images of individual precipitation particles in free fall can be recorded by a planar array CCD camera, the size, shape, orientation are determined from the images, the fall velocities are determined from the time interval between two exposures and displacement of particles simultaneously; the drop size distribution, drop velocity distribution, and precipitation intensity can be estimated by time integration. VPS can detect the hydrometeor from as small as 0.1 mm up to 20 mm with a resolution of 0.1 mm (size), 0.1 $m s^{-1}$ (velocity), 0.1 $mm h^{-1}$ (precipitation intensity).

During May 2013, several rainfall events were observed by VPS at Nanjing, China. Time series and statistical distributions of the particles collected during this period are discussed in this paper. The observations have shown that the VPS can record the sharp images of raindrops in free fall, the data processing algorithms can calculate the size, axis ratio, fall velocity, and orientation of precipitation particles simultaneously, based on which the precipitation intensity, drop size distribution, velocity distribution, shape distribution, orientation distribution can be estimated. Thus besides the classical data products, a VPS system can produce more refined data products, which are important for interpreting weather radar data, investigating regional precipitation features, and studying the physical process of precipitation.

There are several issues that require further research: (i) the performance of VPS in the natural environment, especially in the windy weather, should be examined thoroughly, and the inverse algorithm should be refined accordingly; (ii) more field experiments of VPS for snowfall and hail should be carried out; (iii) the comparisons of VPS with rain gauges, 2DVD, and PARSIVEL disdrometers can be made in the future.

Acknowledgements. This work is supported by the National Natural Science Foundation of China (Grant No. 41327003, and 41205125). The VPS was developed with support from Ying EnTe environment technique Co. LTD, Nanjing, China.

AMTD
6, 10165–10189, 2013

References

Andsager, K., Beard, K. V., and Laird, N. F.: Laboratory measurements of axis ratios for large raindrops, J. Atmos. Sci., 56, 2673–2683, 1999.

Atlas, D. and Ulbrich, C. W.: Path- and area-integrated rainfall measurement by microwave attenuation in the 1–3 cm band, J. Appl. Meteorol., 16, 1322–1331, 1977.

Barthazy, E., Goke, S., Schefold, R., and Hogl, D.: An optical array instrument for shape and fall velocity measurements of hydrometeors, J. Atmos. Ocean. Tech., 21, 1400–1416, 2004.

Battaglia, A., Rustemeier, E., Tokay, A., Blahak, U., and Simmer, C.: PARSIVEL snow observations: a critical assessment, J. Atmos. Ocean. Tech., 27, 333–344, 2010.

Beard, K. V. and Chuang, C.: A new model for the equilibrium shape of raindrops, J. Atmos. Sci., 44, 1509–1524, 1987.

Chandrasekar, V., Cooper, A. W., and Bringi, V. N.: Axis ratios and oscillations of raindrops, J. Atmos. Sci., 45, 1323–1333, 1988.

Huang, G. J., Bringi, V. N., and Thurai, M.: Orientation angle distributions of drops after an 80-m fall using a 2D video disdrometer, J. Atmos. Ocean. Tech., 25, 1717–1723, 2008.

Jones, B. K., Saylor, J. R., and Bliven, L. F.: Single camera method to determine the optical axis of ellipsoid drops, Appl. Optics, 42, 972–978, 2003.

Joss, J. and Waldvogel, A.: Ein Spektrograph fur Niederschlagstrophen mit automatischer Auswertung, Pure Appl. Geophys., 68, 240–246, 1967.

Joss, J. and Waldvogel, A.: Comments on "Some Observations on the Joss–Waldvogel Rainfall Disdrometer", J. Appl. Meteorol., 16, 112–113, 1977.

Kruger, A. and Krajewski, W. F.: Two-dimensional video disdrometer: a description, J. Atmos. Ocean. Tech., 19, 602–617, 2002.

Löffler-Mang, M. and Joss, J.: An optical disdrometer for measuring size and velocity of hydrometeors, J. Atmos. Ocean. Tech., 17, 130–139, 2000.

Liu, X. C., Gao, T. C., and Liu, L.: A comparison of rainfall measurements from multiple instruments, Atmos. Meas. Tech., 6, 1585–1595, doi:10.5194/amt-6-1585-2013, 2013.

Marzuki, Randeu, W. L., Kozu, T., Shimomai, T., Hashiguchi, H., and Schönhuber, M.: Raindrop axis ratios, fall velocities and size distribution over Sumatra from 2D-Video Disdrometer measurement, Atmos. Res., 119, 23–37, 2013.

Newman, A. J. and Kucera, P. A.: Presenting the Snowflake Video Imager (SVI), J. Atmos. Ocean. Tech., 26, 167–179, 2009.

AMTD
6, 10165–10189, 2013

Pruppacher, H. R. and Beard, K. V.: A wind tunnel investigation of the internal circulation and shape of water drops falling at termina lvelocity in air, Q. J. Roy. Meteorol. Soc., 96, 247–256, 1970.
Saylor, J. R. and Sivasubramanian, N. A.: Edge detection methods applied to the analysis of spherical raindrop images, Appl. Optics, 46, 5352–5367, 2007.
Saylor, J. R., Jones, B. K., and Bliven, L. F.: A method for increasing depth of field during droplet imaging, Rev. Sci. Instrum., 73, 2422–2427, 2002.
Schönhuber, M., Lammer, G., and Randeu, W. L.: One decade of imaging precipitation measurement by 2D-video-distrometer, Adv. Geosci., 10, 85–90, doi:10.5194/adgeo-10-85-2007, 2007.
Thurai, M., Szakall, M., Bringi, V. N., and Beard, K. V.: Drop shapes and axis ratio distributions: comparison between 2D video disdrometer and wind-tunnel measurements, J. Atmos. Ocean. Tech., 26, 1427–1432, 2009.
Tokay, A., Kruger, A., and Krajewski, W. F.: Comparison of drop size distribution measurements by impact and optical disdrometers, J. Appl. Meteorol., 40, 2083–2097, 2001.

AMTD
6, 10165–10189, 2013

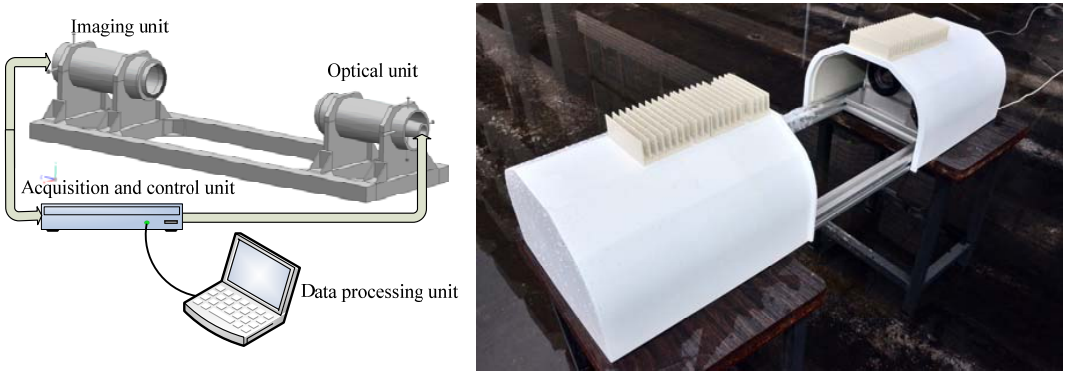

(a) (b)

Fig. 1. The Framework of VPS equipment and a photograph of the prototype VPS.

AMTD
6, 10165–10189, 2013

A video precipitation sensor for imaging and velocimetry of hydrometeors

X. C. Liu et al.

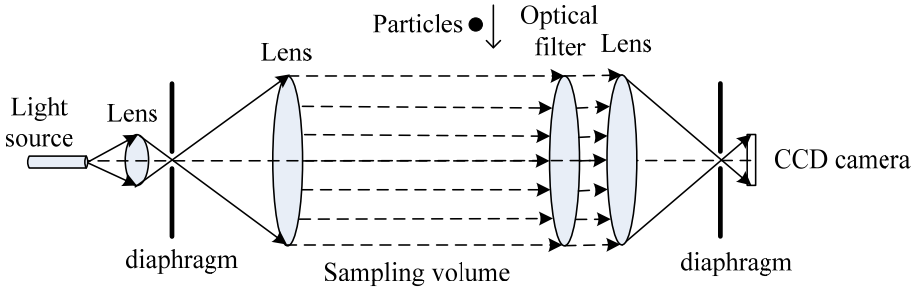

Fig. 2. The schematic diagram of imaging.

AMTD
6, 10165–10189, 2013

A video precipitation sensor for imaging and velocimetry of hydrometeors

X. C. Liu et al.

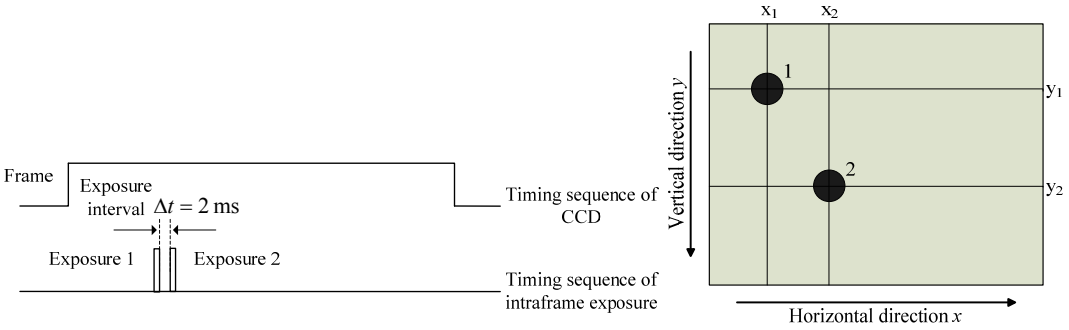

Fig. 3. The timing sequence of exposure and images recorded by VPS.

AMTD
6, 10165–10189, 2013

A video precipitation sensor for imaging and velocimetry of hydrometeors

X. C. Liu et al.

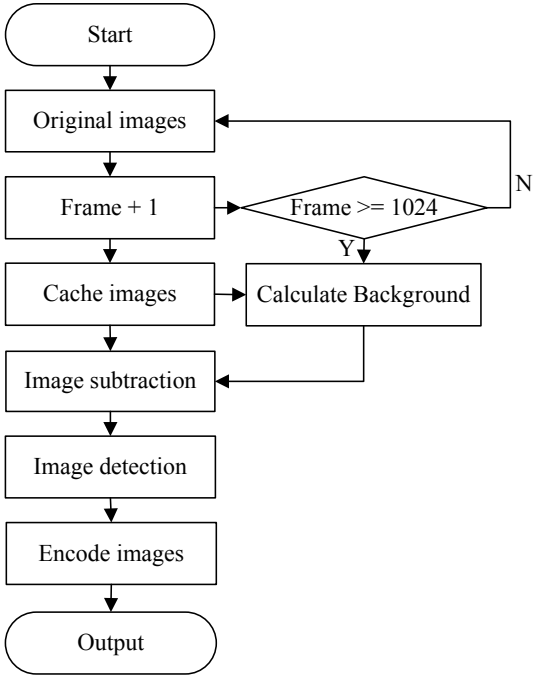

Fig. 4. Flowchart of image background removal.

AMTD
6, 10165–10189, 2013

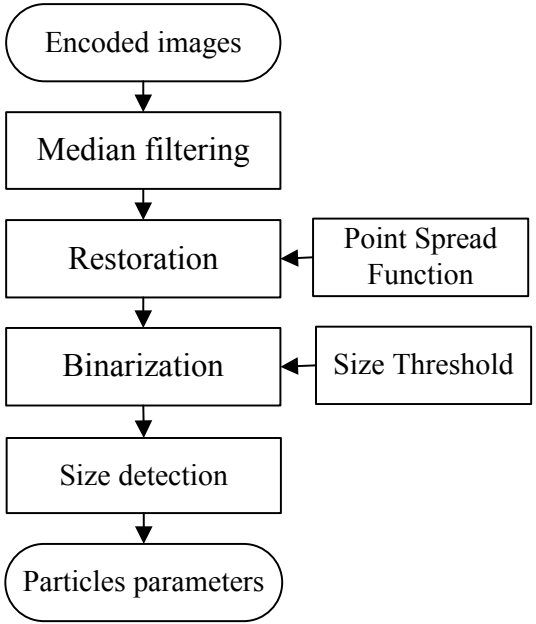

Fig. 5. Flowchart of image processing and feature extraction.

AMTD
6, 10165–10189, 2013

(a) Original images (b) Filtered images (c) Restored images (d) Binary images (e) Particles contour

Fig. 6. Images of a glass ball for calibration (D = 2 mm).

AMTD
6, 10165–10189, 2013

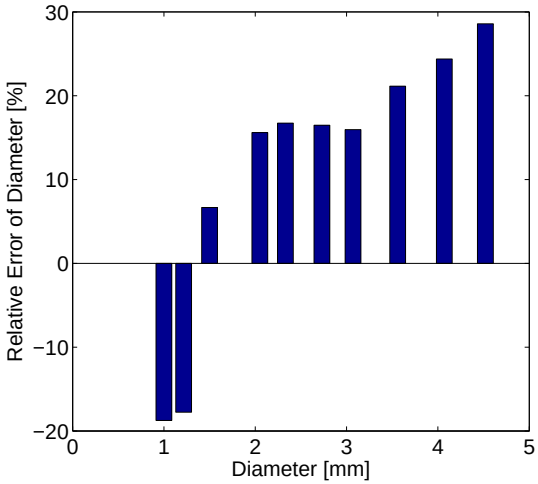

Fig. 7. Relative error of diameter vs. diameter (threshold = 3 %).

AMTD
6, 10165–10189, 2013

A video precipitation sensor for imaging and velocimetry of hydrometeors

X. C. Liu et al.

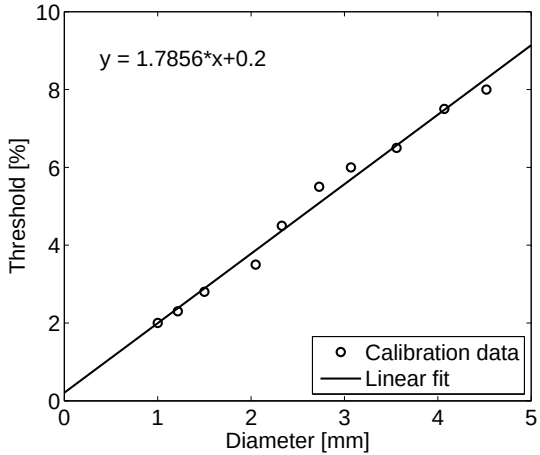

Fig. 8. Plot of binarization threshold vs. diameters for calibration data with linear fit.

AMTD
6, 10165–10189, 2013

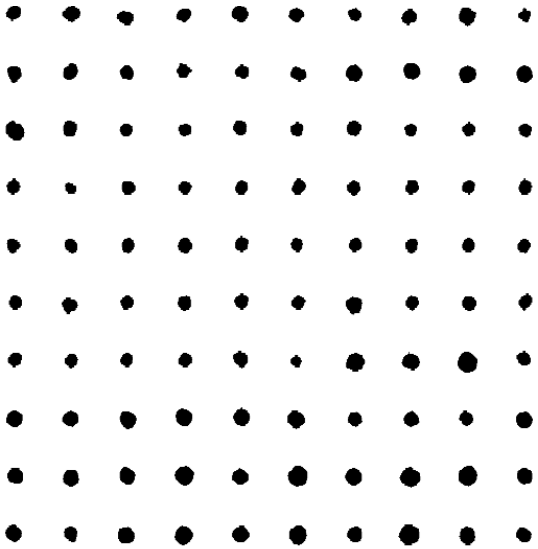

Fig. 9. Samples of images of raindrops in free fall taken by VPS.

AMTD
6, 10165–10189, 2013

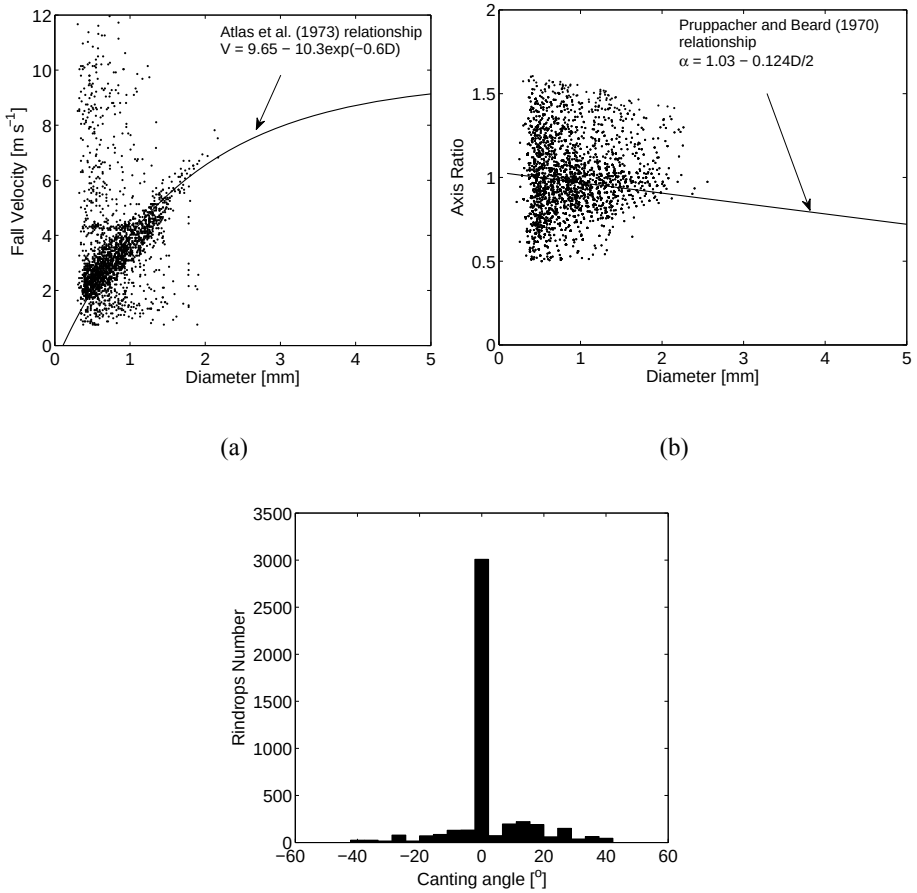

Fig. 10. Fall velocity, axis ratio, and orientation of raindrops observed by VPS.

AMTD
6, 10165–10189, 2013

A video precipitation sensor for imaging and velocimetry of hydrometeors

X. C. Liu et al.

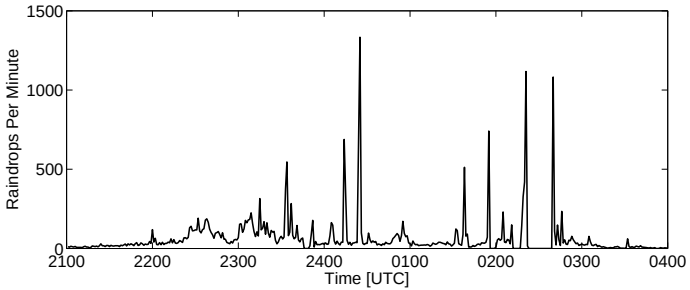

(a)

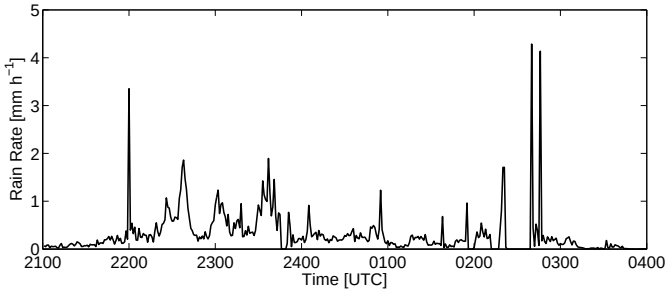

(b)

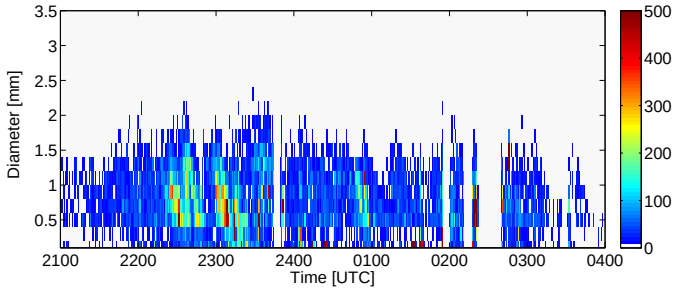

(c)

Fig. 11. History of raindrops observations during a 7 h rainfall event at Nanjing.

AMTD
6, 10165–10189, 2013

A video precipitation sensor for imaging and velocimetry of hydrometeors

X. C. Liu et al.